JVSTB Journal of Vacuum Science & Technology B

Bosch etching for the creation of a 3D nanoelectroporation system for high throughput gene delivery

Paul Bertani, Wu Lu, Lingqian Chang, Daniel Gallego-Perez, Ly James Lee, Chiling Chiang, and Natarajan Muthusamy

Citation: Journal of Vacuum Science & Technology B **33**, 06F903 (2015); doi: 10.1116/1.4932157
View online: http://dx.doi.org/10.1116/1.4932157
View Table of Contents: http://scitation.aip.org/content/avs/journal/jvstb/33/6?ver=pdfcov
Published by the AVS: Science & Technology of Materials, Interfaces, and Processing

Bosch etching for the creation of a 3D nanoelectroporation system for high throughput gene delivery

Paul Bertani[a] and Wu Lu[b]
Department of Electrical and Computer Engineering, The Ohio State University, Columbus, Ohio 43210

Lingqian Chang[a]
Department of Biomedical Engineering, The Ohio State University, Columbus, Ohio 43210

Daniel Gallego-Perez and Ly James Lee[b]
Department of Chemical and Biomolecular Engineering, The Ohio State University, Columbus, Ohio 43210

Chiling Chiang and Natarajan Muthusamy
College of Medicine, The Ohio State University, Columbus, Ohio 43210

(Received 28 June 2015; accepted 21 September 2015; published 7 October 2015)

In order to create a high-throughput electroporation based cell transfection system, it is required that each cell has localized delivery and minimal membrane damage to ensure optimal transfection and longevity post-biomolecule delivery. To meet these requirements, a three-dimensional (3D) nanochannel device was fabricated on a Si platform due its ease of etching, wide industrial availability, and mechanical stability. The device is designed to shoot desired biomolecules into a seated array of target cells to achieve the high-throughput of bulk electroporation, but with greatly reduced cell mortality. To accomplish this, a wafer-scale Bosch etching process was optimized to etch a 3D array of channels consisting of larger microchannels feeding into smaller nanochannels that cells are ultimately seated on for transfection. The microchannel array consists of 50 μm wells spaced 50 μm apart, which are etched from the "back side." The wafer is then flipped over to etch the smaller 650 nm channels on the "front side." In the creation of the 3D silicon device, other feature sizes were explored, and their Bosch etching was characterized for comparison. The results show that when etching samples with the same feature sizes, but different densities, there was no relation between feature density and etch rate for our recipe. However, when etching features, or more specifically, circular channels of different sizes (650 nm–150 μm), the results show a positive correlation with etch rate (1.10–4.06 μm/min). Standard deviations indicate very uniform etching with an average value of 0.1 μm/min across all etches. After optimization, the 3D Si device was tested to ensure successful cell seating and transfection via electroporation, using fluorescence as the tool of evaluation. Fluorescent imaging (postelectroporation) indicates a transfection efficiency of approximately 70% with a cell viability of roughly 90%. © *2015 American Vacuum Society*.
[http://dx.doi.org/10.1116/1.4932157]

I. INTRODUCTION

The manipulation of cells and cellular behavior has become of great interest from a clinical standpoint and may deliver advances in regenerative medicine via cell reprogramming[1–5] and chemotherapeutic delivery into tissue.[6,7] Electroporation is a physical transfection, or delivery, method allowing foreign biomolecules to be introduced into a cell or cell population of interest. This is done using a short, but significantly strong, electrical pulse to porate the cell membrane, resulting in increased permeabilization and the endocytosis of molecules.[8,9] Electroporation is a desirable delivery method due to its simplicity, rapid transfection, minimization of excess chemical components, and controllable operation. Bulk electroporation (BEP) is a commercially available method which involves a large population of cells (millions) suspended in a media between two large (typically plate-style) electrodes for applying the pulses. While effective at delivery, this method can overstimulate cells causing irreversible cell membrane damage and cell death.[10] Cell positioning is also very difficult to control due to the nature of the system, resulting in cells in the same transfection event being exposed to very different electrical potentials.

In an attempt to improve upon the controllability of electroporation-based cell transfection, the introduction of a pore or channel in proximity to target cells has been introduced to both lower the electrical field experienced by the cell as well as localize it. It has been shown that as the channel size is reduced, the more localized electrical field allows biomolecules to be primarily driven into the cell rather than diffusing into the cell.[11] Indeed, a great deal of research has been done on 2D systems making use of a single microchannel setup or a small array (between 5 and 100) channels.[12,13] These systems are excellent for single cell diagnostics and the examination of electroporation-based phenomena. However, they do not have the high-throughput characteristic of BEP. Some systems have integrated microfluidics into

[a]P. Bertani and L. Chang contributed equally to this work.
[b]Electronic addresses: lu.173@osu.edu; lee.31@osu.edu

microelectroporation style devices,[11,14] which increase the number of cells that can be transfected, but not on the scale of thousands to millions at one time. In order to maintain both the high-throughput benefits of BEP and the great controllability and uniform delivery of small channel electroporation, a three-dimensional (3D) silicon nanochannel electroporation system (NES) needs to be designed. Previous work has been done on 3D microchannel based designs that move in the direction of this requirement.[15] Yet, in addition to the merits of microchannel electroporation, nanochannel electroporation has shown higher cell viability and dosage control capability due to the enhanced drive-in delivery.[16,17] Thus, we have designed a 3D cell transfection system, henceforth called the 3D "NES." To create the 3D NES, deep reactive-ion etching (DRIE), or the Bosch process, was employed as the primary method for fabrication. The Bosch process consists of alternating cycles of C_4F_8 and SF_6 plasma to yield an anisotropic etch with smooth side walls and a high aspect ratio.[16–20] The C_4F_8 plasma passivates the silicon (specifically the channel walls) by depositing a thin layer of carbon-based polymer, while the SF_6 is responsible for etching by generating volatile SiF_4. Previous work has shown that Bosch etching has the ability to etch features into silicon varying from hundreds of microns[21,22] to submicron or high nanometer scale.[23–25] While using the same technology, we combine these two different feature size etching processes to create a 3D microfluidic device allowing for cells to be electroporated using a small channel (650 nm), but maintaining 50 μm channels for cargo feeding and giving the device more mechanical stability and user friendliness. During the fabrication of the 3D NES, we explored the etching flexibility of the Bosch process in order to visualize the etch rates and depths if the channel or feature size of the 3D NES were to require alteration for handing cells or cargos of variable sizes.

II. EXPERIMENT

A. Three-dimensional NES fabrication and etching

The device fabrication process, beginning from a thinned silicon wafer, is illustrated in Figs. 1(a)–1(c). The 3D NES was designed as a high-throughput and uniform cellular delivery system with high viability (or very little cell death post transfection). The device works by seating a target cell population in top of the nanochannel opening on the top side of the 3D NES, as shown in Fig. 1(d). Molecules or "cargo" to be delivered are placed on the opposite side of the 3D NES prior to transfection. In order to carry out electroporation, electrodes are placed on the back and front side of the 3D NES. The polarity of these electrodes depends on the charge associated with the cargo or molecules to be delivered. A short (10 ms) pulse was applied to drive the molecules through the microchannels, then the nanochannels, and finally into the cells themselves. The 3D NES was primarily fabricated using conventional photolithography and DRIE etching techniques. Five hundred micrometers thick, double-side polished Si (100) wafers were first cleaned using acetone, isopropyl alcohol, and piranha solutions (H_2SO_4 and H_2O_2 mixture). The wafers were then thinned down to approximately 250 μm by submersion into a potassium hydroxide solution. The thinning process was done at 80 °C and has an etch rate of approximately 1 μm/min. Patterning of small feature sizes (650 nm, 3 μm, and 6 μm) was performed using a GCA 6100C stepper (i-line) in conjunction with AZ-5214 E photoresist to mask all etches in the aforementioned range. All etching work was done with an Oxford Plasmalab 100 system using C_4F_8/SF_6 chemistry only. Alternating cycles of C_4F_8 and SF_6 were set at 7 and 13 s, respectively (100 sccm flow rate for both gases). C_4F_8 cycle time was determined by etch profile viewing. C_4F_8 cycle time was varied until a 90° etch profile and acceptable etch rate are observed. ICP power was set at 700 W for both

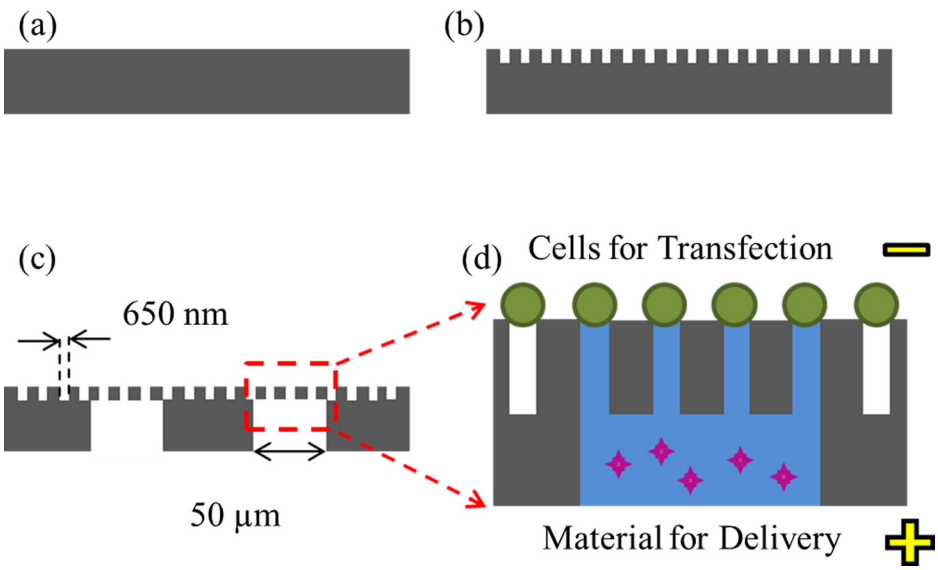

FIG. 1. (Color online) Fabrication process from Si wafer to electroporation. (a) Si wafer thinned to 250 μm, (b) 650 nm nanochannels etched into the top side of the wafer, (c) 50 μm microchannels patterned into the backside of the wafer creating an array of continuous channels, and (d) the electroporation setup illustrating cell seating in preparation for transfection with the desired cargo material.

gases, and RF power was set to 40 and 12 W for SF_6 and C_4F_8, respectively. Etching was done at 30 mTorr and at a temperature of 20 °C. Temperature control was maintained by use of a chiller and LN_2 to ensure temperature deviation was minimized. Twenty standard cubic centimeters per minute helium back-side cooling was also used to assist in this process. Larger feature sizes (15, 50, 100, and 150 μm diameter) were patterned using SPR-220-7 photoresist (10 μm thickness) and an EVG 620 mask aligner. 650 nm, 3 μm, and 6 μm diameter feature sizes were all etched for 15 min, while 15, 50, 100, and 150 μm features were etched for 32 min during characterization. Each processing condition was checked in three areas across the 2 × 2 in. feature region, allowing determination of etching uniformity across the wafer. Etches for final device fabrication are approximately 20 min for the 650 nm channels (depth 23 μm) and approximately 90 min for 50 μm channels (depth 230 μm).

B. Cell handling and electroporation

K562 (human immortalized myelogenous leukemia) cells were used for testing the transfection performance of 3D NES. The cell line was cultured in RPMI 1640 (catalog No. 11875-093), with the addition of 10% (v/v) fetus bovine serum (FBS, heat-inactivated, catalog No. 26010). GATA2 molecular beacon (GATA2 MB, 50 μM/ml, Sigma-Aldrich, excitation/emitting wavelength, 495/515 nm) was used as the fluorescence marker. An inverted microscope (Nikon Elipse Ti) was used to check the fluorescent signal. The nuclei of cells were stained with Hoechst (Sigma-Aldrich, catalog No. 654434, excitation/emitting wavelength, 350/461 nm) to mark the cell location on the chip.

III. RESULTS AND DISCUSSION

A. Bosch etching feature size comparison

Different circular feature sizes were patterned and etched to gain insight on etching phenomena. Using the same patterned area size (2 × 2 in.), trials were conducted using the given etching process on feature sizes varying from 650 nm to 150 μm. This feature range was studied for its relevance to 3D NES design. When fabricating the 3D NES, the 650 nm nanochannel array is necessary for dosage control. The large size range was entertained for feeder microchannels allowing a 3D nanoscale electroporation device to be fabricated with good mechanical stability for ease of handling. Figure 2(a) shows the etch rates for features of 650 nm, 3 μm, and 6 μm in diameter. The etching time for all samples was 15 min. The relationship between etch rate and feature size here is linear and has good uniformity across the patterned area (highest Std. Dev. = 0.031 μm/min). Figure 2(b) shows an SEM image of the 3 μm etching condition result. The etch again appears uniform with very vertical sidewalls. Figure 2(c) evaluates etch rate versus feature size at larger diameters, specifically 15, 50, 100, and 150 μm. Due to the robustness of the SPR-220-7 resist, etching for each of these four cases was carried out for 32 min. The relationship here also appears linear, but with a slightly reduced slope. The etch rates at each point are 2.21, 2.80, 3.07, and 4.06 μm/min for 15, 50, 100, and 150 μm feature arrays,

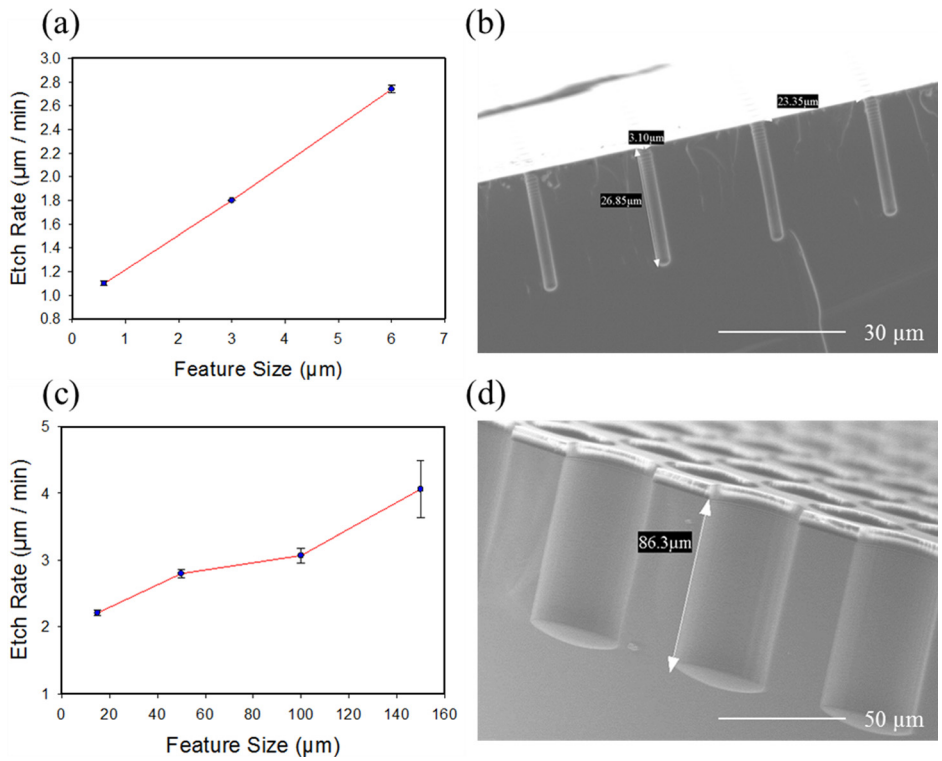

FIG. 2. (Color online) (a) Etch rate vs feature size for 650 nm, 3 μm, and 6 μm circular features. (b) Example etching profile of 3 μm feature array using an etch time of 15 min. (c) Etch rate vs feature size for 15, 50, 100, and 150 μm circular features. (d) Example etch of 50 μm feature array using an etch time of 32 min.

TABLE I. Summary of different feature sizes etched using the Bosch recipe from 650 nm to 150 μm. Feature sizes 650 nm–6 μm were etched for 15 min, while feature sizes 15–150 μm were etched for 32 min.

Feature size	650 nm	3 μm	6 μm	15 μm	50 μm	100 μm	150 μm
Etch rate (μm/min)	1.10	1.80	2.74	2.21	2.80	3.07	4.06
Std. Dev. (μm/min)	0.020	0.001	0.031	0.046	0.067	0.109	0.432
Etch depth (μm)	21.86	27.31	42.87	70.67	86.30	98.23	129.90

respectively. A difference in slope between Figs. 2(a) and 2(c) is observed, which is accounted for by considering the amount of ions and radicals that reach the silicon surface and the difference in etching time. Smaller features (i.e., a smaller opening) make etching more difficult resulting in a lower etch rate. For large feature sizes (15–150 μm), the etching rate dependence on feature size was reduced. This can be attributed to feature sizes becoming sufficiently large so as not to limit the amount of radicals reaching the etching surface, eventually allowing a saturation in etch rate for even larger patterns. Also, during longer etches, the pore depth becomes deep enough to impact etch rate due to the diffusion limited transport process. Results for all etches are summarized in Table I. Standard deviation was calculated as mentioned previously. Based on all etching data, we see that across all etches, there is a positive correlation with feature size and etch rate. This is consistent with what has been reported in the literature, though the etch rate should saturate if the feature size is large enough due to the diffusion limited process.[26,27]

B. Bosch loading effect

Based on the previous section (Sec. III A), we have observed that etch rate is dependent on feature size for our given recipe at feature sizes between 650 nm and 150 μm, with this trend being more pronounced at smaller feature sizes. However, the relationship between the percentage of Si exposed and etch rate has not been evaluated. Concerning Bosch etching and processing, it has been shown that the etch rate is dependent on the percentage of silicon exposed (nonmasked area) on a to-be-etched silicon sample, which is called the loading effect.[28,29] The loading effect refers to the overall influence of the percentage of silicon exposed (nonmasked area) on etch rate.[30] In order to determine the existence (or absence) of the loading effect in our 3D NES etching recipe, three samples with the same feature size (6 μm circular array), but with variable feature densities (15, 25, and 75 μm spacing) were etched. Feature size and sample area (2 × 2 in.) were kept the same, and only the percentage of silicon exposed to plasma and feature density were changed. Figure 3(a) shows the results of the etching test and an essentially constant etch rate as the 6 μm circle pattern density was varied from 15 to 75 μm (center to center distance); thus, a variable percentage of silicon is exposed to plasma. The 15 μm spacing condition corresponds to a value of 12.57% silicon exposed, the 25 μm array a value of 4.52% silicon, and the final 75 μm spacing condition, a value of 0.50%. These densities were chosen to allow for high-throughput transfection, but still keep joule heating low enough as not to impact cell viability. However, all conditions have an etch rate of approximately 2.7–2.8 μm/min. This indicates that the loading effect was not present under these circumstances. However, loading effects might be observed if the percentage of silicon exposed was significantly increased. It is suggested that significant changes in pattern density and/or the percentage of silicon exposed would be required for any noticeable loading effects to occur with this recipe due to the relatively low pressure and high flow rate we are using.[26,31] If the process parameters are altered or the percentage of silicon exposed is sufficiently increased, two results are possible: first, the conditions are such that the amount of radicals present during etching are sufficient as not to limit the etch, in this case, the loading effect will not be observed and the results will be similar or identical to the data seen in Fig. 3(a). Alternatively, the

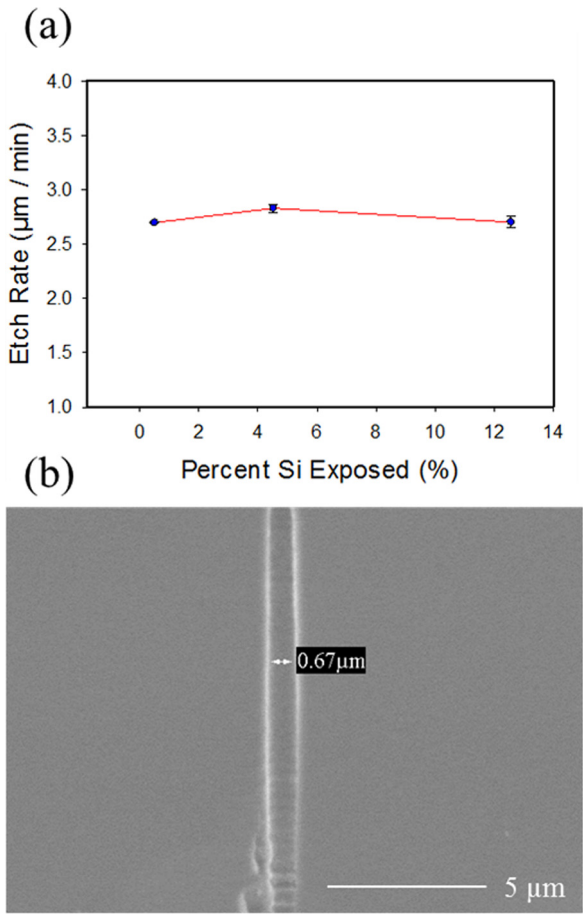

FIG. 3. (Color online) (a) Etch rate vs percent of exposed Si using arrays with identical feature sizes (6 μm) with error bars. (b) Example etch of a single nanochannel feature (approximately 670 nm).

amount of radicals present during the etching process is limited in the diffusion process, and a negative correlation between etch rate and percentage of silicon exposed would be observed (i.e., the loading effect is present). In terms of the 3D NES, the presence of the loading effect is not a large concern as long as the uniformity of the etch across the wafer is good. This allows the nanochannels and microchannels to all connect at the same point during the final etch. Figure 3(b) shows an example of a single 650 nm pore etched during characterization. Pertinent values such as the percentage of silicon exposed, etch depth, and the standard deviation are succinctly summarized in Table II. Standard deviation is given for single etches and calculated using three locations in each region (for example, three locations in the 6 and 15 μm spacing area) indicating excellent uniformity, with the worst case scenario being 0.052 μm/min). Based on these results, the relationship between etch rate and percentage of silicon exposed appears independent for our 3D NES Bosch etching recipe.

C. Three-dimensional NES fabrication and electroporation

Finally, the 3D NES chip fabrication process was completed, and the device was fabricated. Figure 2(d) shows the backside etch of 50 μm microchannels for the first 32 min used in the characterization above. Figure 4(a) shows an SEM image of the fabrication process further along as the etched nanochannel array is clearly observed with the 50 μm channel (undergoing the etching process) approaching them. A distance of 81.7 μm was needed to complete the device in this case and enables channel connection. Figure 4(b) shows a snapshot of the final device cross-section taken by SEM. The front side nanochannel array has made connection with the 50 μm microchannel array. Multiple effective nanochannels are accounted for using only one 50 μm microchannel as shown.

We finally evaluate the performance of the 3D NES system for high-throughput cell electroporation. For our performance test, we use a GATA2 MB for delivery into living K562 cells (a human myelogenous leukemia cell line) for proof of principle and investigating the expression level of GATA2 mRNA in cytosols. The GATA2 molecular beacons are designed with both fluorescent and quencher elements; this allows for the opening of the hairpinlike structure in the presence of the complementary DNA sequence. This opening separates the fluorescence element from the quencher element, allowing a fluorescent signal to be observed. Mutations and overexpression of the GATA2 gene have been linked to leukemia. Detection of GATA2 is thus of great significance for the study of the hematopoietic stem cells. Here, the idea was to prove the device is capable of performing successful electroporation with uniform, high-throughput transfection along with good cell viability. The GATA2 molecular beacons are thus "driven" into the cell via electroporation using the 3D NES. The molecular beacons then open up and bind to the GATA2 present within the K562 cells. This opening of the beacons allows the attached fluorescent molecules to be optically observed. In the experiment, K562 cells were seated on the nanochannel openings (top-side), with GATA2 MB's loaded into the microchannels on the bottom side of the 3D NES. To achieve efficient cell trapping, we applied dielectrophoresis (DEP) force to trap cells onto the nanochannel array reported in previous work.[32,33] Briefly, polarized particles like cells experience a translational dielectrophoretic force when exposed to an electric field. Depending on the difference of permittivity and conductivity between target cells and the physiological buffer solution, cells are attracted or repelled along the direction of the electric field depending on frequency. Using the Clausius–Mossotti equation, simulation results suggest that when using a sucrose solution with a conductivity of approximately 0.03 S/M a positive DEP (pDEP) force was exerted when the frequency was roughly between 100 kHz and 100 MHz.[34] Experimentally, a custom power

TABLE II. Summary loading effect investigation using 6 μm feature at variable center-to-center array spacing. Etching time was 15 min.

Region spacing (μm)	Etch depth (μm)	Etch rate (μm/min)	Percentage of Si exposed (%)	Etch rate Std. Dev. (μm/min)
15	40.52	2.70	12.57	0.052
25	42.50	2.83	4.52	0.037
75	40.46	2.68	0.50	0.004

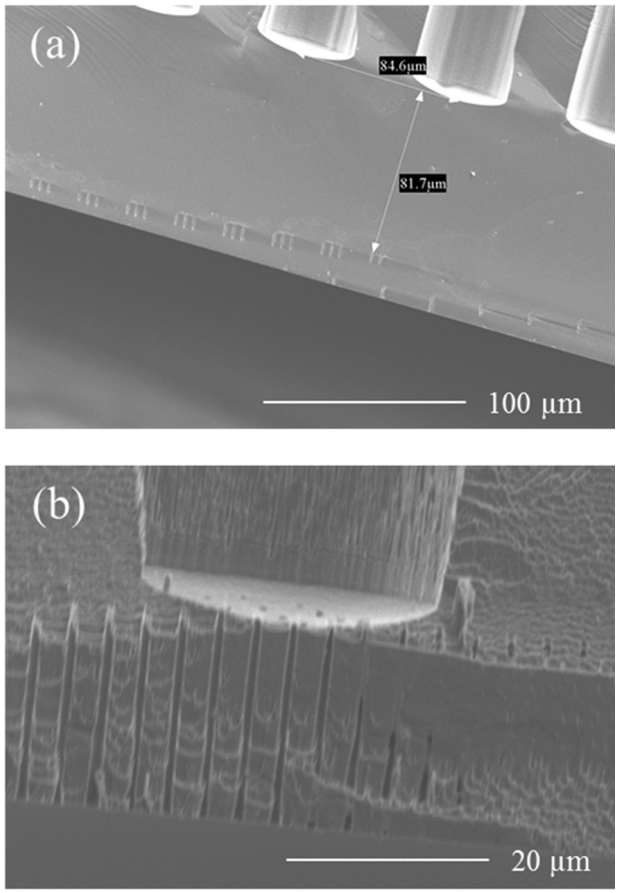

FIG. 4. (a) Electroporation device during fabrication with ~82 μm to go until (b) connection achieved, where the microwells and nanopores meet to form a continuous channel array.

supply was connected to the top electrode and the bottom electrode used for electroporation, with manual switches used to switch from DEP to NEP (Nanoelectroporation) power after cell trapping. The frequency of pDEP moves cells toward the nanopores using a 100 V (peak–peak voltage) nonpolarized square signal with a frequency of 100 kHz. Under these DEP conditions, we achieved efficient cell alignment with the nanochannel array, which was indicated by a DAPI (4′,6-diamidino-2-phenylindole) nuclei stain [Fig. 5(a)]. NEP conditions were applied and GATA2 MBs were delivered into the K562 cells. Strong green fluorescence (from GATA2 MB signal) was observed 1 h after NEP [Fig. 5(b)], which demonstrates expression of GATA2 mRNA in K562 cells. With assistance of pDEP, a transfection efficiency of ~70% and a cell viability of 90% are achieved simultaneously. The high percentage of GATA2 positive cells, on the other hand, validated the high transfection efficiency benefited by the NES platform.

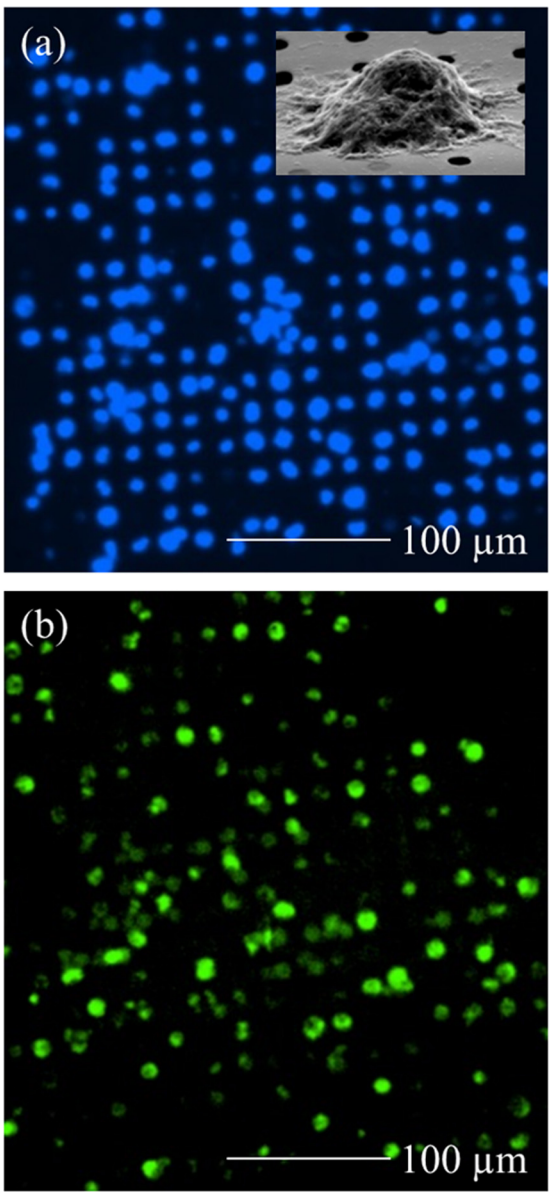

FIG. 5. (Color online) (a) Cell seating on the nanochannel array observed via DAPI staining for visual confirmation (inset). SEM image of a single cell loaded onto the 3D NES surface prior to electroporation. (b) GFP (Green fluorescent protein) fluorescence of the cell population after transfection via electroporation.

IV. SUMMARY AND CONCLUSIONS

A Bosch DRIE etching process has been optimized and characterized for the purpose of fabricating a 3D nanochannel electroporation system based on a silicon platform. The 3D NES allows for high-throughput, efficient, and high cell viability transfection. The Bosch etching processes were characterized in terms of etch rate versus both the percentage of silicon exposed and feature size. The correlation between etch rate and feature size (more specifically channel diameter) is clearly observed with a stronger correlation shown at smaller feature sizes as compared to larger ones. The percentage of silicon exposed is varied between 0.50% and 12.57% for 6 μm feature arrays. The results indicate that this Bosch etching process has an etch rate of 2.8 μm/min which is independent of the percentage of silicon exposed during the etching of micropore arrays. Different results may be observed when changing parameters specific to the Bosch process (feature size, flow rate, pressure, etc.). The 3D NES system was then evaluated for effective cell seating/trapping and efficient cell transfection using fluorescent imaging for confirmation of successful GATA2 delivery into K562 cells. One hour after transfection, the results show that the GATA2 MB, K562 cells display strong green fluorescence indicating successful transfection by the system with good uniformity. Final quantitative analysis shows approximately a 70% transfection efficiency with a cell viability of approximately 90% (or around 10% cell death).

ACKNOWLEDGMENTS

The authors thank the National Science Foundation (EEC-0914790) for supporting this study.

[1]F. Soldner *et al.*, Cell **137**, 1356 (2009).
[2]A. Rosa and A. H. Brivanlou, Cell Stem Cell **7**, 549 (2010).
[3]N. S. Bhise, K. J. Wahlin, D. J. Zack, and J. J. Green, Int. J. Nanomed. **8**, 4641 (2013).
[4]J. Yu, K. Hu, K. Otto-Smuga, S. Tian, R. Stewart, I. I. Slukvin, and J. A. Thomson, Science **324**, 797 (2009).
[5]B. K. Chou *et al.*, Cell Res. **21**, 518 (2011).
[6]R. Cadossi, M. Ronchetti, and M. Cadossi, Future Oncol. **10**, 877 (2014).
[7]S. Orlowski, J. Belehradek, Jr., C. Paoletti, and L. M. Mir, Biochem. Pharmacol. **37**, 4727 (1988).
[8]E. Neumann, S. Kakorin, and K. Toensing, Bioelectrochem. Bioenerg. **48**, 3 (1999).
[9]S. Y. Ho and G. S. Mittal, Crit. Rev. Biotechnol. **16**, 349 (1996).
[10]M. dal Maschio *et al.*, Nat. Commun. **3**, 960 (2012).
[11]T. Geng and C. Lu, Lab Chip **13**, 3803 (2013).
[12]H. Y. Wang and C. Lu, Anal. Chem. **78**, 5158 (2006).
[13]K. Ø. Andresen *et* al, J. Micromech. Microeng. **20**, 055010 (2010).
[14]M. B. Fox, D. C. Esvald, A. Valero, R. Luttge, H. C. Mastwijk, P. V. Bartels, A. van den Berg, and R. M. Boom, Anal. Bioanal. Chem. **385**, 474 (2006).
[15]L. Q. Chang *et al.*, Small **11**, 1818 (2015).
[16]E. Boukany *et al.*, Nat. Nanotechnol. **6**, 747 (2011).
[17]K. Gao *et al.*, Small **10**, 1015 (2014).
[18]M. Putty and K. Najafi, *Solid State Sensor and Actuator Workshop* (IEEE, Hilton Head, SC, 1994), pp. 213–220.

[19]F. Laerme, R. B. Bosch, A. Schilp, K. Funk, and M. Offenberg, *Micro Electro Mechanical Systems* (IEEE, Orlando, FL, 1999), pp. 211–216.
[20]R. B. Bosch, U.S. patent 4,855,017 (8 August 1989).
[21]A. A. Ayon, X. Zhang, and R. Khanna, Sens. Actuators, A-Phys. **91**, 381 (2001).
[22]S. A. McAuley, H. Ashraf, L. Atabo, A. Chambers, S. Hall, J. Hopkins, and G. Nicholls, J. Phys. D: Appl. Phys. **34**, 2769 (2001).
[23]B. Wu, A. Kumar, and S. Pamarthy, J. Appl. Phys. **108**, 051101 (2010).
[24]M. M. Mirza, H. Zhou, P. Velha, X. Li, K. E. Docherty, A. Samarelli, G. Ternent, and D. J. Paul, J. Vac. Sci. Technol. B **30**, 06FF02 (2012).
[25]X. Wang, W. Zeng, G. Lu, O. L. Russo, and E. Eisenbraun, J. Vac. Sci. Technol. B **25**, 1376 (2007).
[26]Q. X. Zhang, Q. Y. Guo, J. Li, and A. Q. Liu, Int. J. Comput. Eng. Sci. **4**, 303 (2003).
[27]J. Karttunen, J. Kiihamäkia, and S. Franssila, Proc. SPIE **4174**, 90 (2000).
[28]I. Rangelow, J. Vac. Sci. Technol. A **21**, 1550 (2003).
[29]C. J. Mogab, J. Electrochem. Soc. **124**, 1262 (1977).
[30]H. V. Jansen, M. J. de Boer, S. Unnikrishnan, M. C. Louwerse, and M. C. Elwenspoek, J. Micromech. Microeng. **19**, 0033001 (2009).
[31]C. Hedlund, H.-O. Blom, and S. Berg, J. Vac. Sci. Technol. A **12**, 1962 (1994).
[32]R. M. Johann, Anal. Bioanal. Chem. **385**, 408 (2006).
[33]T. Nagai *et al.*, Blood **84**, 1074 (1994).
[34]L. Chang *et al.*, Lab Chip **15**, 3417 (2015).